Characterization of a steamed oil reservoir using cross-well seismology

By BJORN N.P. PAULSSON, MICHAEL E. SMITH, KARLA E. TUCKER, JOHN W. FAIRBORN
Chevron Oil Field Research Company
La Habra, California

Cross-well seismic tomography is developing into an important tool for reservoir management, and within the last few years there have been some notable advances in our understanding its imaging capability. Tomography has evolved from its roots in medicine to encompass a broad range of geophysical applications (which include earthquake hypocenter location, mining, and nuclear waste disposal) in addition to oil field operations. The fundamental technical requirements for the latter have been demonstrated. High-frequency seismic waves capable of traveling long interwell distances can be generated without damaging the borehole, and mathematical inversion techniques can give reliable images as long as problems associated with nonuniform and incomplete sampling are handled correctly.

Cross-well seismology is a broader term which includes, in addition to the tomography discussed above, imaging using cross-well reflections. Only in combining the tomography and reflection techniques will we be able to fully develop the potential of cross-well seismology. Current applications focus on monitoring EOR processes, but perhaps more important is the potential of the method to improve our geologic knowledge of the reservoir. The old concept that oil reservoirs are homogeneous has given way to the realization that they are heterogeneous, complex, and may contain pockets of untapped oil even after many years of production. The US Department of Energy has estimated that 60–70 percent of the mobile oil is left in the ground when a reservoir is considered economically depleted. Much is left behind due to reservoir heterogeneities which effectively compartmentalize the reservoir into a number of isolated oil pockets. Cross-well seismology has been identified by DOE, and also by the oil industry, as a critical technology for identifying the location of this bypassed oil.

So far, most cross-well seismic surveys have been conducted for the purpose of mapping steam zones in steam-enhanced oil recovery operations. Seismology is well suited for this application since the presence of live steam in the reservoir sharply reduces *P*-wave velocity. Moreover, for low-gravity oils in poorly consolidated sand reservoirs, the seismic *P*-wave velocity decreases significantly with increased temperature. Consequently, seismic velocities can in principle be used as a measure of reservoir temperature and/or an indicator of live steam within the reservoir.

Midway-Sunset is one of a number of oil fields in the San Joaquin Valley of central California that are characterized by low-gravity oil and shallow, unconsolidated reservoir rocks. Many, including Midway-Sunset, have undergone years of steam drive to enhance oil recovery. Although most of these programs have been successful, there are common problems—poor sweep efficiency, gravity override, and steam channeling through zones of high permeability. Foam can be used to reduce injected gas mobility in steam drives if early gas breakthrough occurs at producing wells due to either gravity override or viscous fingering. Mechanisms of gas mobility reduction with foam have been studied both theoretically and experimentally by various investigators. In order to better understand foam behavior under reservoir conditions, Chevron conducted a steam foam mechanistic field trial in the Midway-Sunset field. The test's objectives were to establish how foam propagated away from the injection well, the impact of foam on the steam-swept pore

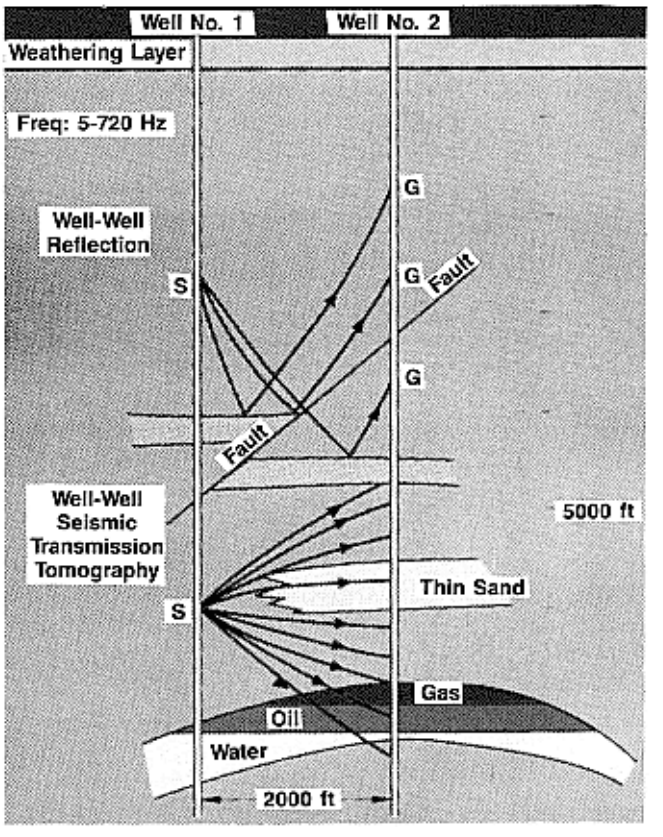

Figure 1. The concepts of cross-well seismology showing how both reflected and direct events can be used to define detailed structure and stratigraphy.

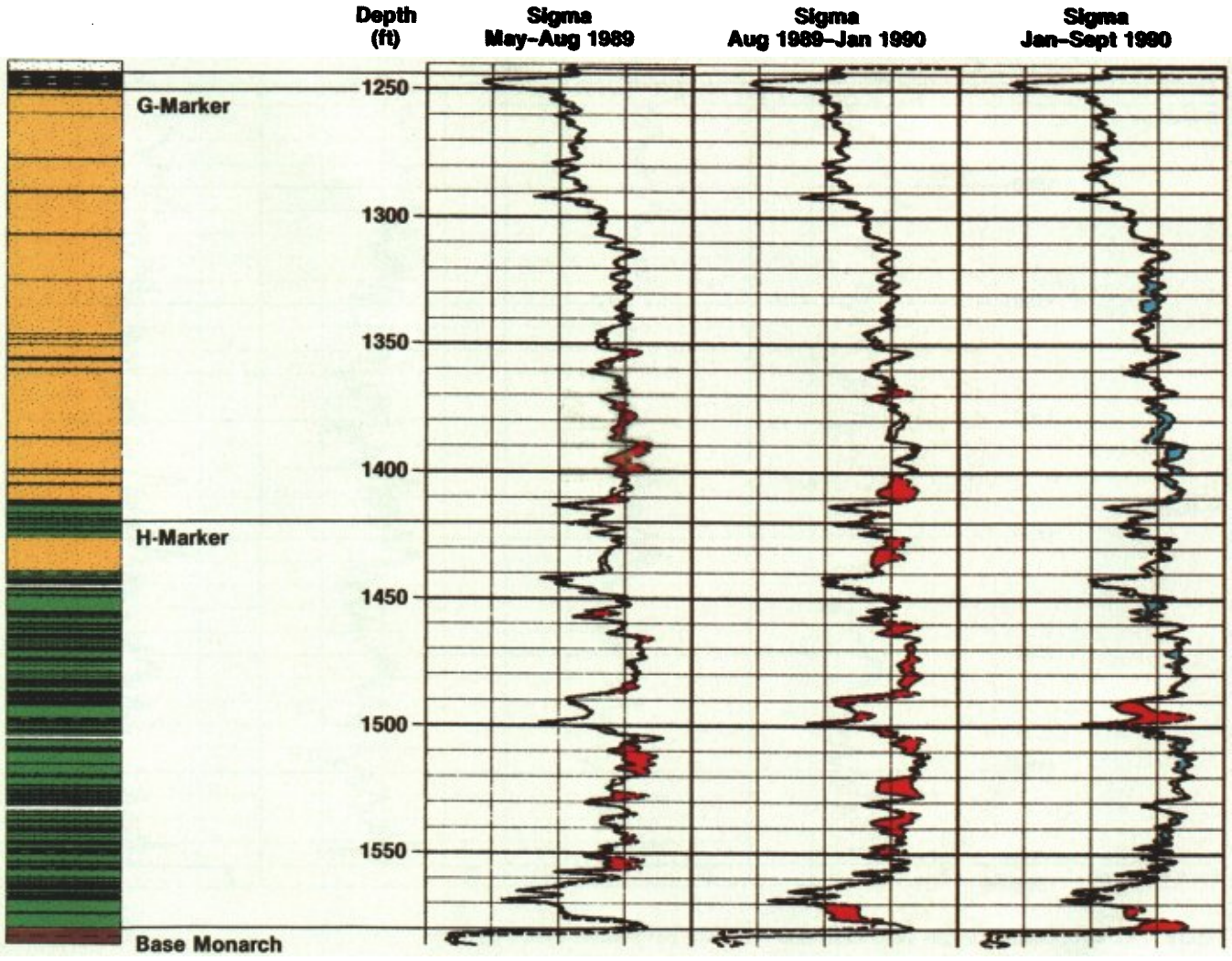

Figure 2. Relative changes in gas saturation (red = gas saturation increase, blue = gas saturation decrease) in OW3 using the Sigma trace from Schlumberger's TDT-P (pulsed neutron capture) log.

volume, and how much incremental oil was produced.

Naturally, it is important to establish the location of the steam zone during the course of the steam drive and to determine the effectiveness of the foam injection in altering any undesirable steam movement. Traditionally, observation wells are drilled to monitor reservoir pressure, temperature, and gas saturation. In 1988 three observation wells were directionally drilled in the 68BW pattern with bottomhole locations shown in Figure 5. The injection well, 68BW, is about 40 ft from the closest observation well, OW1, and 70 ft from observation well OW4. OW3 is a twin well to OW1, located at a slightly greater distance from 68BW. OW1 was perforated and completed with a rod pump and pumping unit to allow periodic fluid sampling for detection of the surfactant front and to allow pressure monitoring. OW3 and OW4 were not perforated and were intended for temperature and gas saturation (TDT) logging. Schlumberger's TDT-P log was run periodically in OW3 and OW4 to allow calculation of changes in steam vapor saturation based on change in neutron capture cross-section (Sigma) response. Well OW3 was continuously cored through the reservoir interval (980–1558 ft). The core was described and routine core analysis completed on one-inch diameter plugs taken at 1 ft intervals.

Observation wells are expensive and measure parameters at only one location. A complementary method which extends information away from the observation wells to other areas of the reservoir is therefore desirable. Since seismic velocities are a sensitive function of temperature and phase of the reservoir fluids and since surface seismic data is of very poor quality at Midway-Sunset, we conducted two cross-well seismic tomography surveys to monitor changes in the steam chest.

This paper discusses the results of the time-lapsed cross-well tomography surveys at Midway-Sunset. The first cross-well survey, conducted in July 1989 (prior to significant foam injection), was done to provide a first mapping of the steam chest. Steam injection into the pattern had started in 1982 and a considerable steam chest had developed. The second survey was conducted in August 1990, 14 months after foam injection commenced, and after significant changes were seen in the observation and producing wells.

Before discussing the survey, however, we would like to point out some advantages of cross-well seismic data over surface data. Figure 1 illustrates the typical cross-well geometry. The first clear advantage is that both the source and receivers are below the attenuating weathered layer. B.N.P. Paulsson and J.M. Harris independently showed in 1988 that when source and receivers are below the weathered layer, frequencies of 700–2000 Hz can be recorded in fluid-saturated sediments. This is more than an order of magnitude greater than the upper limit which can be recorded on the surface. On the other hand, the maximum frequency we have seen propagated through massive steamed or gas-saturated zones is well below 400 Hz. A second advantage is that in traveltime tomography, which is what this article discusses, we measure the arrival times of the direct

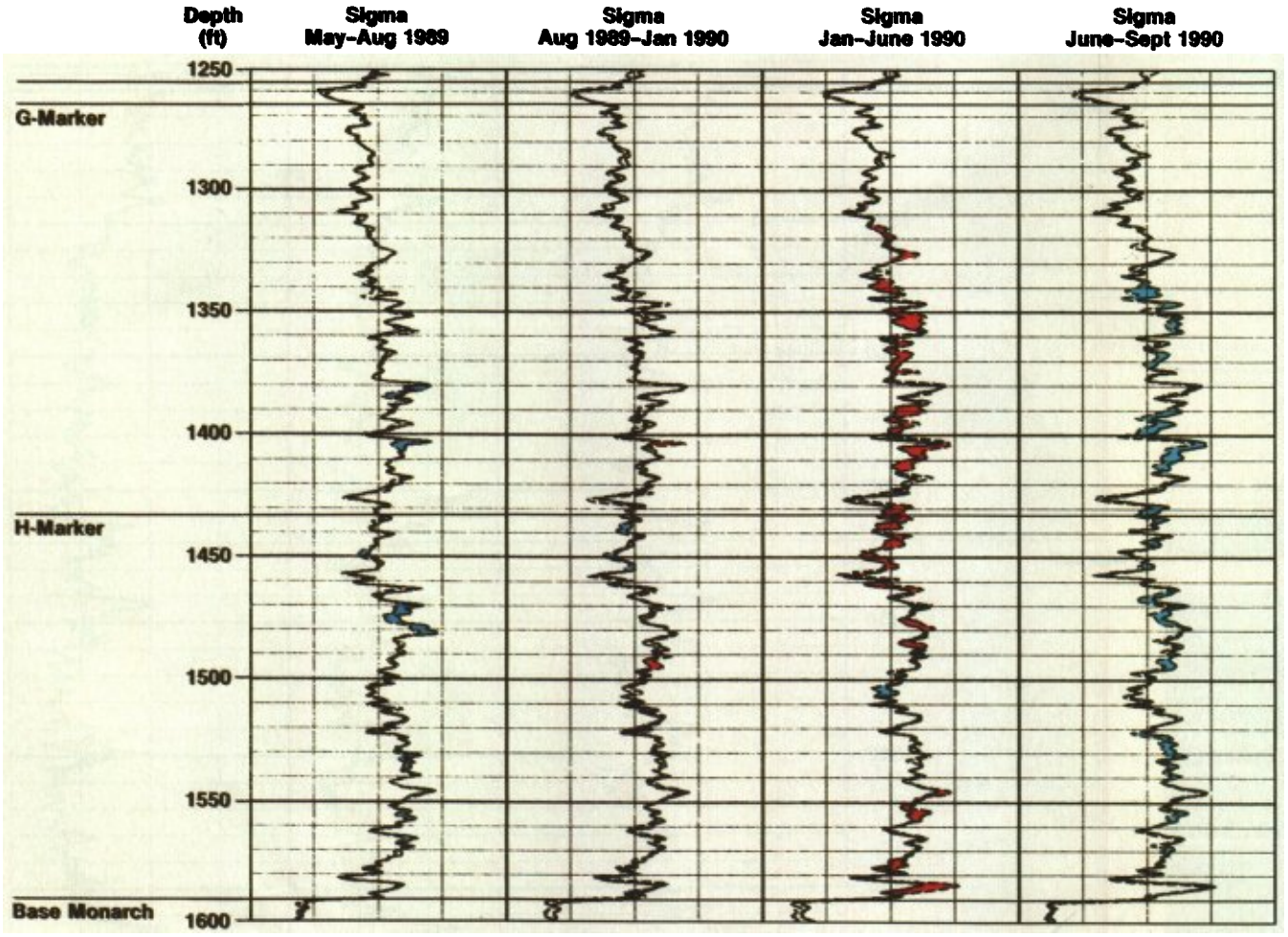

Figure 3. Relative changes in gas saturation in OW4 (same parameters as in Figure 2).

transmitted *P*-wave. This is generally the highest amplitude event on the seismogram. Conversely, we measure reflections on conventional surface data and they are severely attenuated by reflection losses as well as transmission losses through the weathered layer. However, as will be pointed out later, we do see reflections on cross-well data and some can be quite strong. This is because the borehole environment is very quiet, and the source and receivers are much closer to the reflector. These reflections contain a great deal of information, and we are currently incorporating them into our tomographic inversions process.

Geology. Midway-Sunset is one of a group of oil fields which lies in a series of northwest-southeast trending anticlines on the west side of the San Joaquin Valley. The specific study area (68BW pattern) overlies a local small syncline that plunges to the east, so the updip (maximum dip = 10°) direction influencing steam migration ranges from north-northwest to south-southwest. Production in section 26C, 32S, 23E is from the poorly consolidated upper Miocene Monarch sandstone, a member of the Monterey formation. Oil gravity is 13 API, and parts of the section were placed on steam drive as early as 1975 after an extended period of primary production and cyclic steam-enhanced recovery.

The Monarch sandstone is composed of a series of turbidites and debris flows of variable thickness and grain size that reach a maximum total thickness of 500–600 ft in the study area. The sequence coarsens upward from thinly interbedded sandstones, siltstones, and diatomaceous mudstones deposited in a medial to distal position on the fan to massive conglomerates and sandstones with few interbedded mudstones deposited in a proximal position on the fan or in the channel feeding the fan. In general, the interbedded mudstones are less disturbed and more laterally continuous in the lower part of the sequence because the turbidites are finer grained and the environment is quieter in the distal portion of the fan. The mudstones in the upper portion of the sequence, however, were often disturbed or eroded out completely during the emplacement of the coarser-grained, high-energy turbidites in the proximal part of the fan. Thus, survival of continuous mudstones over any substantial area is less likely in the upper part of the section.

Although porosity and permeability are slightly higher in the finer-grained, better-sorted turbidites of the lower part of the sequence, the vertical permeability is much higher in the massive, amalgamated, coarser-grained turbidites of the upper part of the sequence. This results in better sweep efficiency above the H-marker than below.

Figures 2 and 3 compare relative gas saturation before the start of steam-foam injection and several months later. The response in OW3 (January 1990) is first and greater than the response in OW4 (June 1990) because it is closer to the injection well. Although there is no visible barrier on logs or in the core from OW3 between 1310 ft and the G-marker, no steam override has been observed. This may be due to a thin mudstone that is present in the injection well at this horizon, but is not correlatable to OW3. Steam override is beginning to occur in OW4, however, where gas/steam saturation is approaching the G-marker. The increase in fluid saturation in the last period between June and August 1990 shows the effects of some of the field

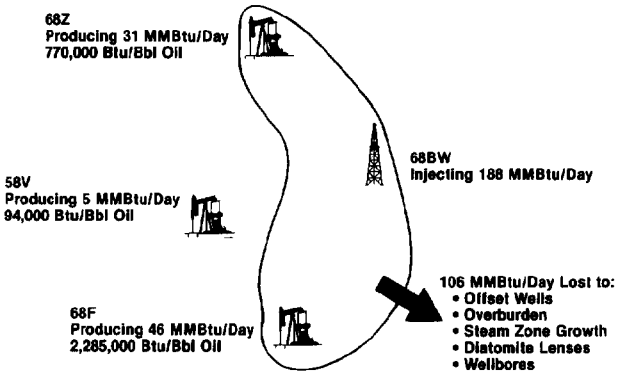

Figure 4. Outline of steam front in 68BW steam drive pattern based on temperature observation logs 10 months before cross-well seismic survey.

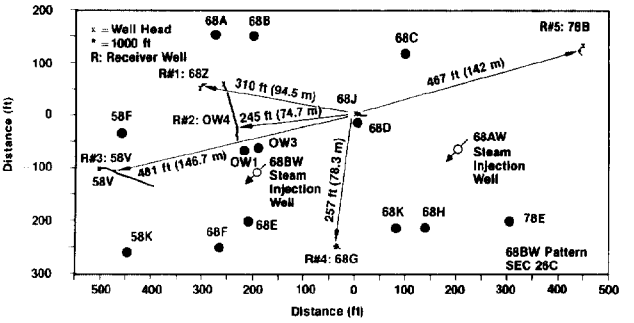

Figure 5. Map view of cross-well survey site in 68BW pattern.

operational difficulties encountered. The steam injection was down for a substantial period during this time, which led to a relative increase in the fluid saturation due to a collapse of the steam chest.

Survey description. Figures 4 and 5 are plan views of the survey area. Figure 4 shows the steam injection well, 68BW, and the outline of the steam chest as of August 1988. These data were developed by conducting an interwell tracer program using tritiated water to track the steam vapor and liquid phases, along with sulfur hexafluoride to determine the vapor-phase-only connectivity. The elongated pattern indicates a preferred steam course in a north-south direction. In an attempt to even out the mobility differences, and consequently the steam chest, foam was added to the steam.

The geometry of the cross-well survey is shown in Figure 5. Source well, 68J, is located to the east of the steam chest of primary interest. Three of the five receiver wells (68Z, OW4, and 58V) are either within or on the other side of the steam chest relative to the source well. The fourth receiver well, 68G, is to the south where the cross-well section (68J-68G) was not expected to include the steam chest in the first survey. Therefore, this would provide a background velocity which was not affected by high temperature or steam. The fifth receiver well, 78B, was only used for the second survey in August 1990. This cross-section was, however, critical for correct interpretation of the results of the other cross-well surveys.

Steam was injected between the depths of about 1350 and 1580 ft in 68BW. The tomography survey was designed to image the depth interval from 1000 ft to the base of the Monarch sandstone, about 1600 ft. The source depths for the tomography surveys ranged from 1000-1560 ft in 20 ft intervals. The receiver depth intervals were also 20 ft. The actual receiver locations varied slightly in each well because of the difference in total depths, but the range of receiver depths was close to that of the source. This resulted in a 29-source × 31-receiver tomography survey.

The receivers were three-component, borehole-clamping geophones. The source for the first survey was an 80 in^3 Bolt air gun which has been used extensively for cross-well surveys in the San Joaquin Valley. The downhole air gun for the second survey had three 40 in^3 chambers.

Although the Bolt air gun is satisfactory for *P*-wave tomography surveys, it does have shortcomings for recording later arrivals such as shear waves and reflections. The major problem is tube waves generated by the air gun. They propagate up and down the source well with very little attenuation and generate secondary body waves at every borehole discontinuity. In low-velocity sediments, these tube waves can also generate conical waves in a manner somewhat analogous to Mach waves from supersonic aircraft. Secondary waves generated at the bottom of the well will dominate the seismogram and obscure everything underneath it. However, at least they are easy to recognize; the secondary waves that are generated at small discontinuities along the well bore are much more difficult to recognize and, consequently, make interpretation of the later arrivals difficult and uncertain.

Another problem we encountered was the quality of the data which were characterized by low S/N ratios, mainly due to large gas saturations in the pattern, and had little or no energy above 300 Hz. To increase the useful seismic energy and increase the S/N ratio of the data, a hydraulic vibrator that clamps to the borehole wall and transmits energy into the formation by reacting against an axial vibrating reaction mass is under development. In order to test the vibrator and compare it to the air gun, we recorded a fan of cross-well data using both sources at a depth of 700 ft. (These data have been discussed in *Characterization of a shallow steam oil reservoir using cross-well seismology* by Paulsson and J.W. Fairborn, published in the *Proceedings* of the 19th Annual Convention of Indonesian Petroleum Association, 1990.) In general, we see much higher S/N ratio data (more than 20 dB higher) with the vibrator for *P, S,* and reflection arrivals in these highly attenuating sediments. This observation is supported by results found by other researchers in terms of effectiveness of radial versus axial sources.

Tomographic inversion and results. The inversion was performed using a standard Algebraic Reconstruction Technique (ART). The principle behind ART is similar to other inversion processes: namely, to determine a model that minimizes the difference between some observed property and the corresponding property calculated from the model. In our case, the observed property is *P*-wave direct arrival times, and the model is the distribution of *P*-wave velocity.

The velocity model is characterized by rectangular boxes, or pixels, in which the velocity must be calculated. The pixel size is determined by the source and receiver spacing and must be such that each pixel is traversed by many rays. For the geometry at Midway-Sunset, we chose a pixel size equal to the source and receiver spacing (20 ft). This spacing is small enough to obtain tomograms which can be used for interpreting gross saturation and lithology changes, but not small enough to detect bedding-scale (1-5 ft) changes in saturation or lithology.

The structure of the tomographic solution is that each raypath represents one equation of traveltime as a function of the unknown pixel velocities. Since there are more traveltime equations than pixel velocities, the set of equations is overdetermined and can be readily solved. Conventional methods solve all the equations simultaneously, usually by least squares. ART differs in this respect; it solves one equation at a time by modifying the velocities of all the pixels traversed by the ray in some prescribed way. Since the pixels are

traversed by many rays, the average of all the modifications turns out to be a good estimate of the correct one. The advantage here is one of computational efficiency. The difference between ART and Simultaneous Reconstruction Techniques (SIRT), one other commonly employed tomographic inversion method, is that SIRT takes the more conventional route and solves for all the traveltime equations simultaneously. Some researchers have reported less success with ART than with other techniques. We, however, find that ART, correctly used and with proper modifications, is a fast and stable inversion routine.

The inversion proceeds in two iterative loops, which begin with some user-supplied guess at the velocity model. We have found that the final result is not sensitive to this initial guess and that a simple constant-velocity model is satisfactory for starters. The outer loop computes the traveltimes for this starting model; the inner ART loop then modifies the velocity model to minimize the difference between the observed and computed times. Control then passes back to the outer loop which recomputes the traveltimes for the new model and so forth. Iteration is required because this inner loop assumes a linear relationship between model perturbation and traveltime change. The assumption is good as long as the perturbations are small. However, the assumption fails as the model changes get large, so the traveltimes have to be reevaluated by ray tracing in the outer loop. That is, one ART loop allows for small changes, while the ray trace loop allows ART loops to combine and make large changes. The process is repeated until some convergence criteria are reached (which in this case is no further reduction in traveltime differences).

One way to improve the resolution significantly is to add the cross-well reflections into the analysis of cross-well seismic data (as shown in *The McKittrick cross-well seismology project* by Paulsson et al., *SEG Expanded Abstracts* 1990). For wavelengths of 10 ft (assuming 700 Hz recorded data with a formation velocity of 7000 ft/s), we can map the top and the bottom of individual beds as thin as 2.5 ft. We anticipate that the future direction of cross-well seismology will include both tomographic *P*- and *S*-wave velocity and attenuation inversions as well as reflection analysis to accurately map the location of bed boundaries and of gas-fluid interfaces.

Using ART, the *P*-wave velocities were determined in each 20 × 20 ft pixel, smoothed, contoured, and then color-coded to form the displays shown in Figures 6-9. In the 1989 tomograms (Figure 6), the low velocities (red and purple) that traverse the steam zone stand out in sharp contrast to the higher velocities between the 68J and 68G wells (where the steam zone was not present in the 1989 survey).

There are three important interpretive features on the tomograms from 1989. The first is the location of the steam zone. It is much closer to well 58V than originally thought (recall Figure 4) and indeed steam breakthrough was observed in well 58V just prior to the survey in July 1989. There is, however, an apparent mismatch between the size of the low velocity zone in the 58V-68J and the OW4-68J cross-sections. A better match would have shown the low-velocity zone in the first cross-section extending further to the right (east). This mismatch is due to the low resolution near the bottom of the 58V-68J cross-section where the data were particularly poor. The second observation is the lack of severe vertical spreading of the steam moving away from the injector, a common and deleterious occurrence in areas where there is good vertical permeability. The thin diatomaceous mudstone layers apparently contain the steam within the reservoir beds. However, some gravity override did occur in an updip direction; note how the top of the high T/low S_o zone rises updip from 68G to 58V to OW4 to 68Z. The third observation is the low-velocity zone in the vicinity of the source well, 68J, between about 1000 and 1200 ft. This interval had been on production for many years and the low velocity reflects the undersaturated conditions. The reservoir at this depth is above the water table, so the produced oil is replaced by gas, not liquids. Higher velocities, and presumably higher oil saturation, exist away from 68J, suggesting the possibility of vertically expanding the steam drive. This vertical expansion was initiated in 1991.

In summary, the 1989 survey was able to map the location of the steam. This mapping contributed to a better understanding of the steam distribution and to a new model of its behavior in the thinly interbedded sandstones and diatomaceous mudstones in the lower part of the injection interval of the 68BW well.

Figure 7 shows the results from 1990. The four cross-sections in this figure are the same as in Figure 6. It is apparent that many changes in the velocity field have occurred. The following are the most significant:

1. A large low-velocity zone developed between depths of 1200 and 1400 ft in all cross-sections.
2. A high-velocity zone developed between depths of 1425 and 1475 ft centered around the 68J well.
3. The low-velocity zones seen in the bottom left of the images in Figure 6 decreased in size; this is especially apparent in the section 68Z-68J.
4. Velocities decreased substantially in the bottom right hand corner of the section 68J-68G.
5. Velocities decreased in the upper left hand corner in cross-sections 68Z-68J and OW4-68J.

The first of these changes, the velocity decrease between 1200 and 1400 ft, is the most conspicuous. Figure 8 shows the results from subtracting the 1989 *P*-wave velocity images in Figure 6 from the 1990 images in Figure 7. In Figure 8, the yellow and red fields represent a velocity decrease and the green and blue fields a velocity increase. A velocity decrease can be interpreted qualitatively as an increase in the temperature and/or in the gas saturation, and a velocity increase can be interpreted as a decrease in the temperature and/or gas saturation. We most likely have coupled processes. This makes interpretations of the velocity changes a non-trivial exercise.

At first it was not clear why we had a decrease in the *P*-wave velocities at these depths. It appeared that the steam from 68BW was mainly confined to below 1400 ft as seen in Figure 6. It was fortuitous that we added the fifth cross-section, 68J-78B, to the second survey. Figure 9 shows the combined cross-well images from 58V-68J and 68J-78B. The image from the latter clearly shows the large, low-velocity zone and how it connects with the low-velocity zones seen in Figure 7. The mis-tie at 68J above 1220 ft is most likely due to the directional nature of well 58V (Figure 5), and the attempts to correct for this in the cross-well seismic data were not entirely successful.

The combined results from the post-foam surveys seen in Figure 7 and Figure 9 clearly indicate the steam is coming from the 68AW steam injector. This has also been confirmed by an increased interwell connectivity between 68AW and 68J, measured by a reduction in tracer arrival times. The reason for the shallower position of the steam from the 68AW pattern is that the top of the injection interval in 68AW is stratigraphically 30 ft higher (closer to the G-marker) than in the 68BW well. In addition, the G-marker barrier is discontinuous between the two adjacent patterns, which allowed the steam to migrate higher stratigraphically into the more massive, amalgamated coarse-grained turbidites above the G-marker. This explains the difference in the behavior of the steam between the two injection wells and indicates the complex dynamics we have between different and adjacent steam injection patterns.

The second and the third of the changes seen in Figures 7 and 8 are the increase in the velocities (green and blue colors in Figure 8) below 1300 ft. We interpret the large increase in the *P*-wave velocity seen centered around the 68J well as an effect of resaturation of the sediment by the cooling water injected into well 68J to keep the downhole air gun operational. However, the resaturation of the formation by the injected water does not entirely explain the large velocity increases below 1300 ft (particularly near wells OW4 and 68Z). Note also that the velocity increase is greater at 68Z than OW4 and that 68Z is also further away from the injector well. This suggests that the foam is having the desired effect of decreasing steam mobility. Recalling that the purpose of the foam injection was to control high-permeability channels, we can infer that we indeed see evidence that the foam had an effect on the steam in the formation

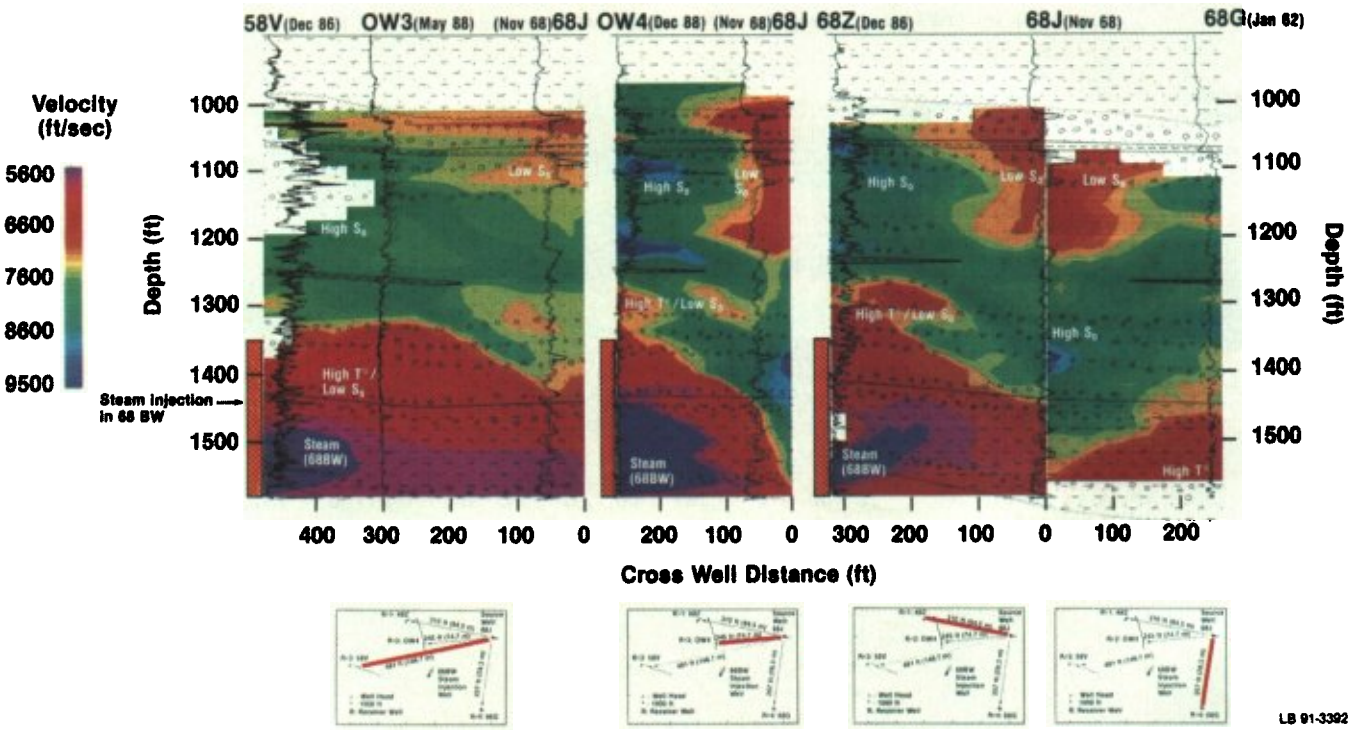

Figure 6. Four tomographic *P*-wave velocity images recorded between source well 68J and receiver wells 58V, OW4, 68Z, and 68G. Cross-well seismic data recorded prior to foam injection in July 1989. Logs displayed are resistivity.

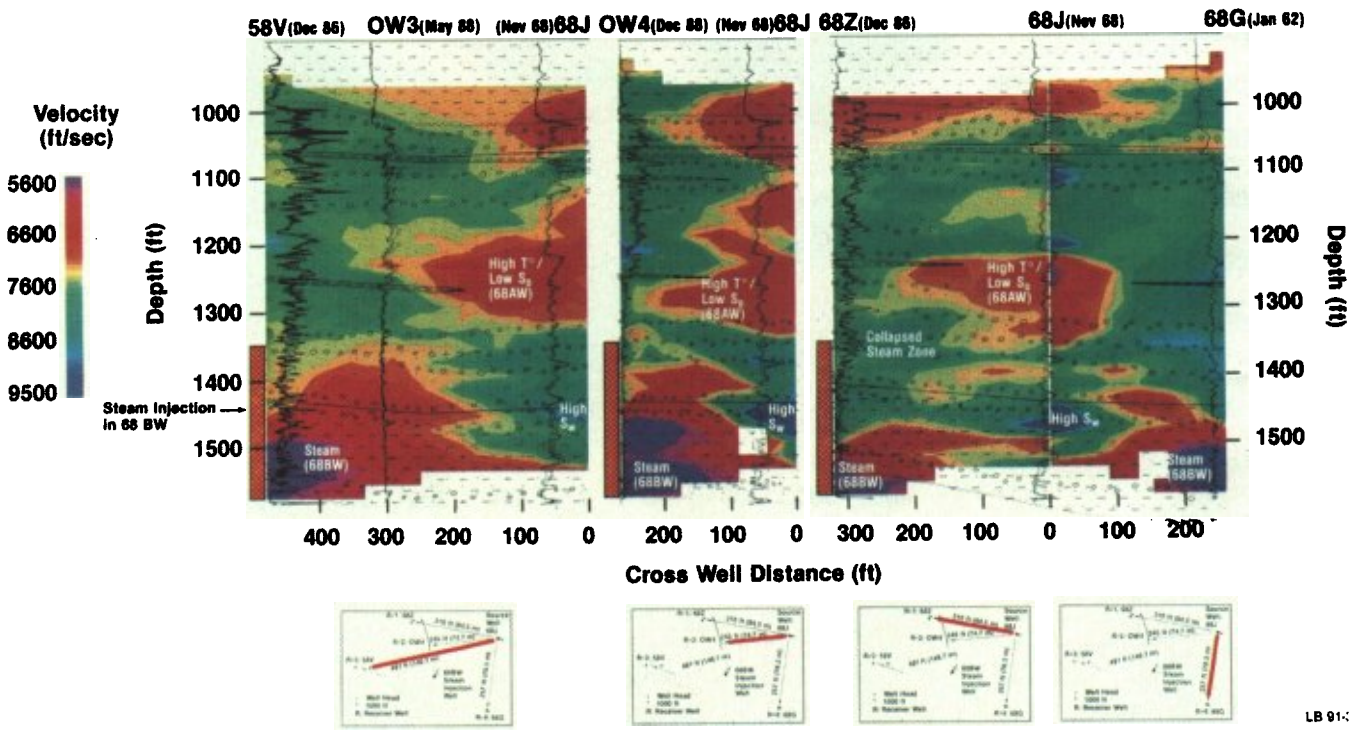

Figure 7. Four tomographic *P*-wave velocity images recorded between source well 68J and receiver wells 58V, OW4, 68Z, and 68G. Cross-well seismic data recorded in August 1990 after one year of foam injection. Logs displayed are resistivity.

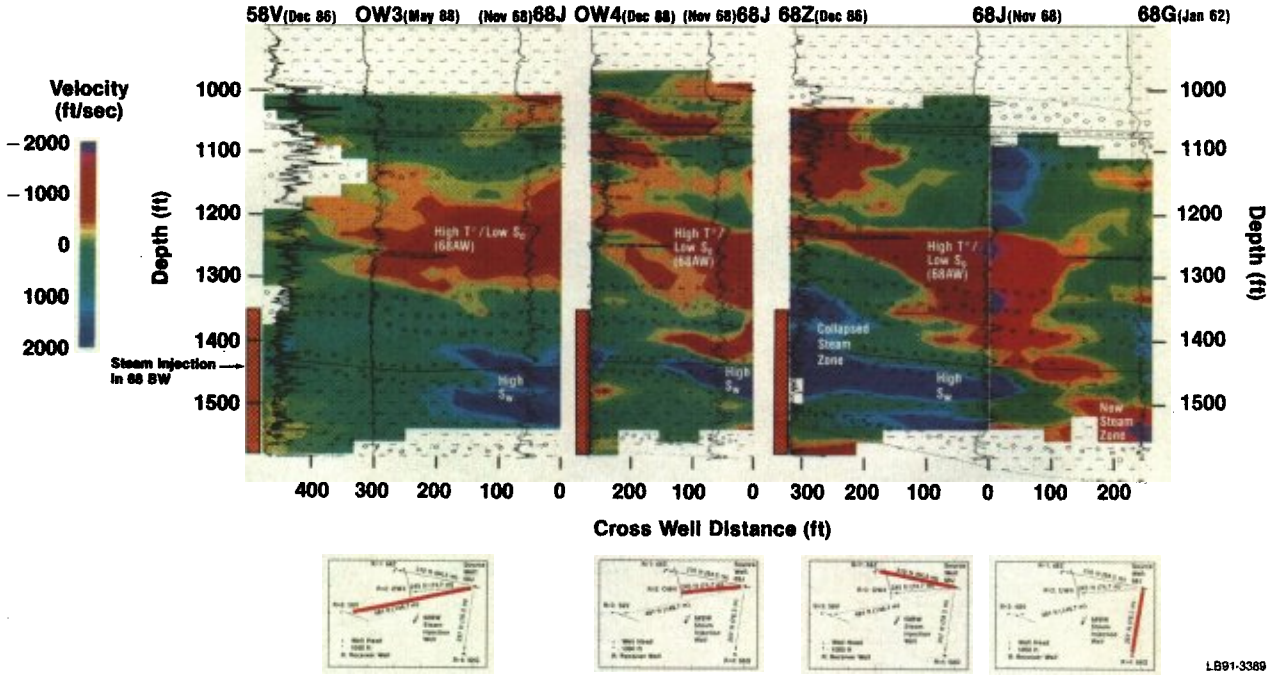

Figure 8. Four differential tomographic *P*-wave velocity images. The images were obtained by subtracting the velocities imaged in 1989 from the velocities imaged in 1990. Logs displayed are resistivity.

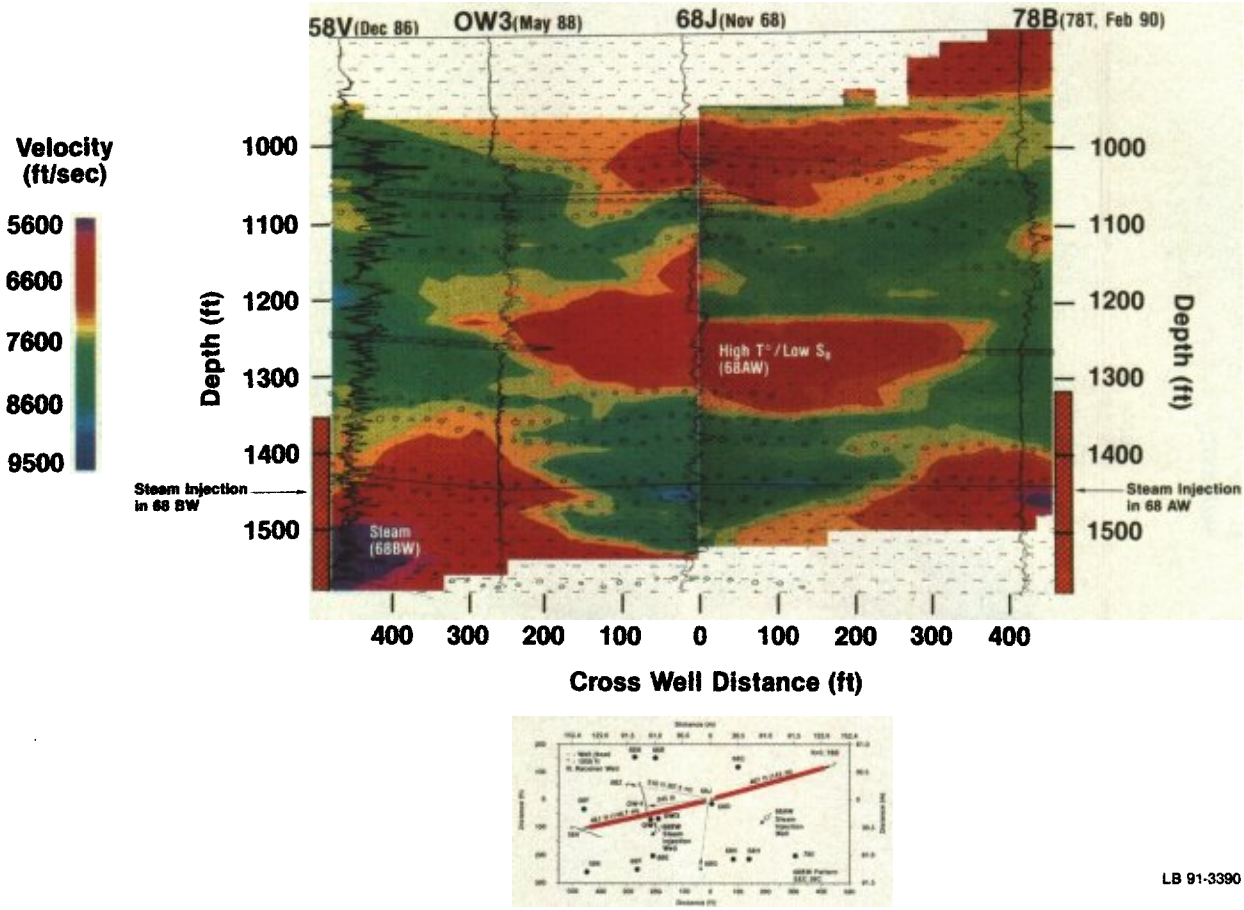

Figure 9. Two tomographic *P*-wave velocity images recorded between source well 68J and receiver wells 58V and 78B. These data were recorded in August 1990. Logs displayed are resistivity.

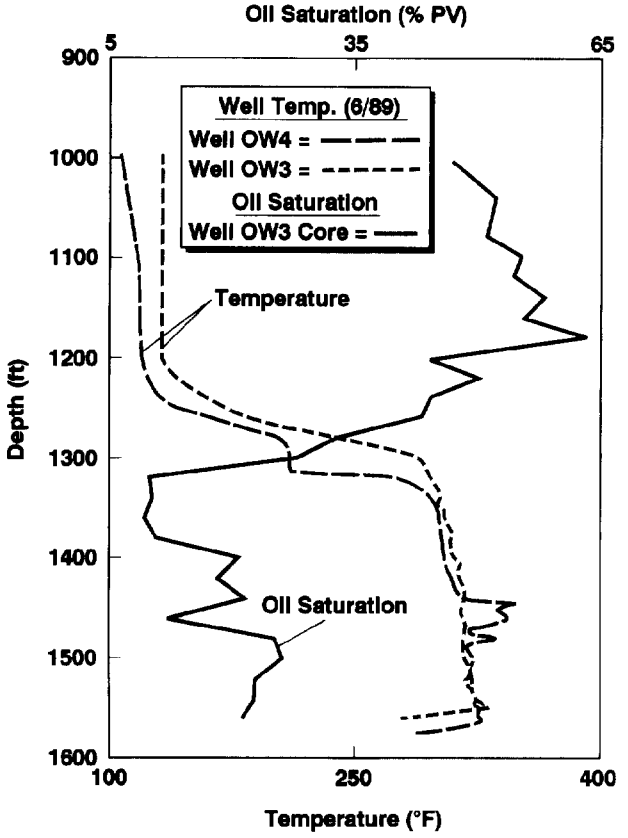

Figure 10. Graph of oil saturation and temperature versus depth as observed by analysis of core from OW3 and temperature monitoring in OW3 and OW4.

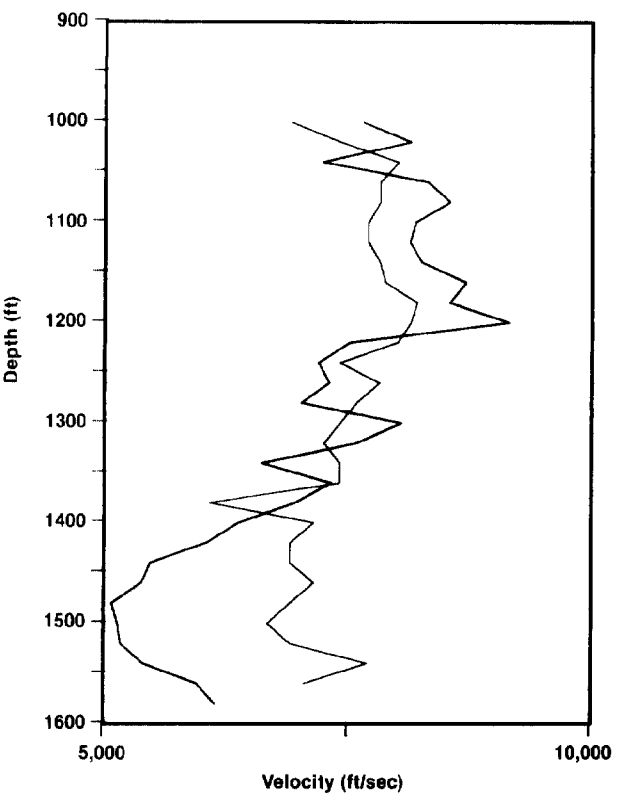

Figure 11. Well log velocity and tomogram velocity adjacent to well OW4 as a function of depth. Well log velocities are averaged over 20 ft intervals. Note the general correlation between decrease in tomographic velocities and decrease in oil saturation shown in Figure 10. The well log was acquired in December 1988 and the cross-well survey in July 1989.

several hundred feet from the injector well by plugging the high-permeability channels near the injector well.

There are, however, some complicating factors. During the month before the second cross-well seismic survey in 1990, operational problems with the steam injection caused substantial downtime. This could have caused the steam chest to collapse and consequently increase the velocity. At present we cannot resolve this ambiguity and simply accept it as an alternate interpretation.

The fourth of the cited changes in the velocity field is the decrease seen in the lower right hand corner of section 68J-68G. This is most likely caused by an increase in the steam chest in the direction of the 68G well from the 68BW injector. This could have been aided by the foam injection.

The fifth of the changes in the velocity fields is the decrease seen in the upper left hand corner of OW4-68J and 68Z-68J. We do not, at this time, have a good explanation for the changes seen in this part of the section. In all images, the uppermost low-velocity zone is related to the section above the Monarch, which was probably never oil saturated.

Relationship between temperature, oil saturation, and *P*-wave velocity. The top of the Monarch sandstone, around 1000 ft, is clearly seen on all logs which are shown alongside the tomograms in Figures 6-9. Originally, oil saturated the entire section from 1000 ft to the base of the Monarch sandstone (1560-1600 ft), but decreased resistivity on the dual induction log in wells completed in the 1980s indicates the section below about 1250 ft has been depleted. As mentioned, production in this interval has been enhanced by steam drive. The effectiveness of the steam drive can be seen in Figure 10, which shows oil saturation and temperature plotted as a function of depth. These data were taken from observation wells OW3 and OW4. The strong correlation between oil saturation and temperature indicates that the steam drive was effective in enhancing oil production. Figures 6 and 7 show confinement of the steam below 1310 ft in OW3. This is 50 ft below the G-marker and does not correlate with any noticeable change in lithology in the core. However, this confinement is substantiated by both temperature and saturation data seen in Figure 10.

Although the 1989 images show high T/low S_o for the injection interval, a considerable amount of bypassed oil remained in the lower part of the interval. Oil and rock can heat up without creating gas, so the assumption that high temperature leads to higher gas saturation is not always correct. The oil saturations in general, however, are higher overall in the upper interval, between the top of the Monarch and the G-marker (1000-1270 ft), than in the injection interval.

The data also indicate that the seismic *P*-wave velocity is related to temperature and therefore to oil saturation. Figure 11 shows *P*-wave velocity versus depth determined from the sonic log in OW4 and a vertical cross-section of the tomogram near (second column of pixels away from the well) OW4. Sonic log velocities were averaged over 20 ft intervals to have the same apparent resolving power as the tomogram velocities.

The *P*-wave velocities from the tomograms, shown in Figure 11, change gradually from a depth of 1200 to 1500 ft, while both the temperature and the saturation changes mainly occur from a depth of 1200 to 1300 ft. The resulting scatter in crossplots between

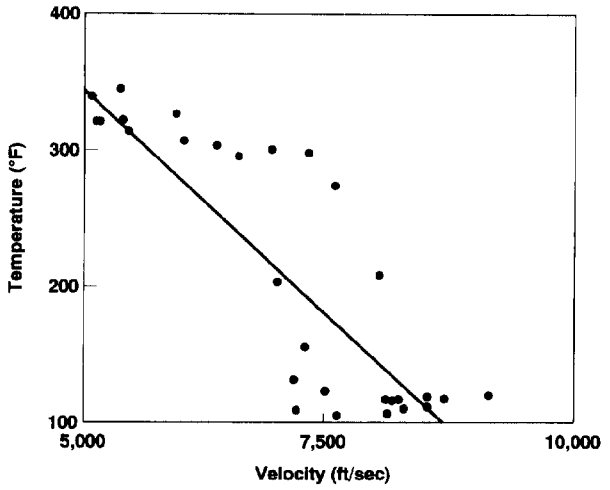

Figure 12. Crossplot of tomogram velocities near the OW4 well, Figure 11, and temperatures from well OW4, Figure 10. Note the general decrease of velocity as the temperature is increased.

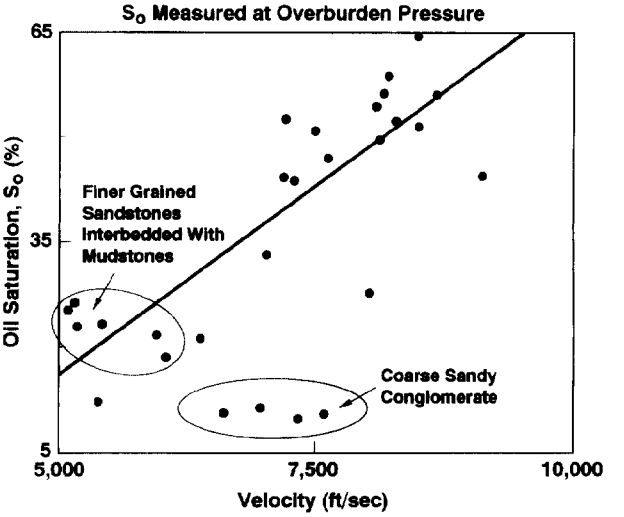

Figure 13. Crossplot of tomogram velocities near OW4, Figure 11, and oil saturation estimates from well OW3 core, Figure 10. Note the increase in velocity as oil saturation increases.

P-wave velocities and temperature and oil saturation are most likely due to the variable lithology and oil saturation (Figures 12 and 13). The velocity difference between coarse-grained turbidites in the upper section (high) and interbedded fine-grained turbidites in the lower section (low) also contributes grossly to this trend of high-to-low velocity with depth. Coarse-grained turbidites have a higher density and lower porosity than fine-grained turbidites and diatomaceous mudstones.

In reservoirs consisting of heavy oil and poorly consolidated sediments, there is an ambiguity between the effects of gas in the pore spaces and elevated temperature, since both would decrease the *P*-wave velocity. The reservoir at Midway-Sunset is above the water table, so gas, as well as condensed steam, replaced the produced oil. Consequently, we are seeing the combined effects of high temperature, steam, and oil production. The high velocities in the shallow parts of the Figure 7 tomograms are low temperature and high oil saturation areas. The low velocities, on the other hand, indicate areas of high temperature and/or lower oil saturation either because steam has been driven through them or because they have already undergone long periods of primary production.

Conclusions. Cross-well seismic tomography has proved to be a suitable technique for monitoring thermal EOR processes in shallow, low-gravity oil fields such as Midway-Sunset. Seismic velocity is a sensitive function of both reservoir temperature and the presence of gas. Since the heat front affects the amount of oil produced, we can say that seismic velocities are a qualitative measure of the oil saturation and that the velocity tomograms of Figures 6, 7, and 9 could also be represented, in a qualitative way, as cross-sections of oil saturation.

We found, in the two surveys we recorded, very large changes in velocities due to both steam injection and water injection. This indicates that the reservoirs are very dynamic in nature and that they respond very quickly to injection and production. Cross-well seismology therefore could be used to assess various production and stimulation strategies without spending the time involved in waiting for a production response. It would, however, have been much easier to interpret the tomograms if the time between surveys had been a few (2-3) months rather than 14 months. A shorter time between surveys could be critical for a detailed understanding of the behavior of the reservoir.

The borehole air gun is satisfactory for *P*-wave cross-well tomography; however, a different source is needed for interpreting later arrivals, such as shear waves and reflections or having high enough S/N ratio of the *P*-waves to make attenuation tomography feasible. It is also clear from the results in these surveys that more data need to be collected. A 30 × 30 or 50 × 50 survey over the cross-sections discussed in this paper simply will not sample the reservoir enough to resolve individual beds. We need to look at surveys which are on the order of 100 × 100 (10 000 rays) to 200 × 200 (40 000 rays). The only practical way to reach these data volumes is with multilevel receiver strings with 100 levels or so. To deal with the 3-D effects of reservoirs and the resulting data complexities, we also need the receiver arrays to be directional. That is the same as saying that the multilevel receiver strings need to be three-component, oriented, and clamped. This is a formidable design challenge for the future. However, while this new source and receiver technology is being developed, much good work can be done with existing sources, geophone and hydrophone arrays.

It is, however, not enough to do successful cross-well seismic surveys and image the cross-well velocity distribution and the location of bed boundaries. The geophysical work needs to be integrated with the work of engineers and geologists. For production geophysics to become a generally used technique, geophysical information has to result in improved management of our hydrocarbon reservoirs. Only a direct positive effect on the bottom line will keep geophysics relevant for production problems.

Suggestions for further reading. *Elastic properties of unconsolidated porous sand reservoirs* by S.N. Domenico (GEOPHYSICS 1977). *Steam foam mechanistic field trial in the Midway-Sunset field* by F. Friedman et al. (presented at SPE's Western Regional Meeting in Long Beach, California, 20-22 March 1991). *Cross-well seismic measurements in sedimentary rocks* by J.M. Harris (*SEG Expanded Abstracts* 1988). *A three-component downhole seismic vibrator* by B.N.P. Paulsson (*SEG Expanded Abstracts* 1988). *Monitoring of thermal EOR fronts by seismic methods* by C.A. Tosaya et al. (SPE paper 12744, presented at SPE's California Regional Meeting, 1984). LE

Acknowledgment: We would like to thank Chevron Oil Field Research Company and Chevron USA for the opportunity to do this work and for allowing us to publish the results.